

Old open clusters: UBGVRI photometry of NGC 2506[★]

G. Marconi¹, D. Hamilton², M. Tosi³, A. Bragaglia³

¹ *Osservatorio Astronomico di Monte Porzio, Italy, e-mail marconi@coma.mporzio.astro.it*

² *Institut für Astronomie & Astrophysik, Universität München, München, Germany, e-mail hamilton@mpia-hd.mpg.de*

³ *Osservatorio Astronomico di Bologna, Italy, e-mail angela@astbo3.bo.astro.it, tosi@astbo3.bo.astro.it*

ABSTRACT

UBGVRI photometry for the open cluster NGC 2506 is presented. From comparison of the observed colour-magnitude diagrams with simulations based on stellar evolutionary models we derive in a self consistent way reddening, distance, and age of the cluster: $E(B-V)=0-0.07$, $(m-M)_0 = 12.6\pm 0.1$, $\tau = 1.5-2.2$ Gyr. The cluster shows a well definite secondary sequence, suggesting that binary systems constitute $\gtrsim 20\%$ of the cluster members visible in the colour-magnitude diagram.

Key words: Hertzsprung-Russell (HR) diagram – open clusters and associations: general – open clusters and associations: individual: NGC 2506

1 INTRODUCTION

This paper belongs to a series devoted to the study of supposedly old open clusters, which represent one of the best possibilities to study the chemical and dynamical evolution of our Galaxy. Open clusters provide unique information on the chemical abundances and gradients in the disc (e.g., Janes 1979, Panagia and Tosi 1981, Friel and Janes 1993); on the average stellar ages and radial velocities at different galactic radii (e.g., Janes and Phelps 1994, hereinafter JP94); and on the interactions between thin and thick discs (e.g., Sandage 1988). In addition, they are the only class of objects covering a large range of distances (several kpc around the Sun) and ages (from a few Myr to $\gtrsim 10$ Gyr) and can, therefore, tightly constrain galactic evolution theories. Furthermore, in order to avoid misleading effects, it is mandatory to work with very accurate observational data and to treat them homogeneously (see Section 5, and e.g. Carraro and Chiosi 1994a, hereinafter CC94, Friel 1995).

In order to obtain this kind of homogeneity and to be able to study accurately the metallicity and age distribution of open clusters with galactocentric distance, we are analyzing systems of different ages and metallicities, located at different galactic radii. To this end, we have obtained deep photometry for several clusters, and have supplemented these observations with published data of comparable quality to ensure a sample as large as possible of uniformly derived ages, metallicities and distance moduli.

These quantities are derived from comparison of the

observed colour-magnitude diagrams (CMDs) to synthetic ones generated by a numerical code based on stellar evolution tracks and taking into account theoretical and observational uncertainties (Tosi et al. 1991). These simulations are much more powerful than the classical isochrone fitting method to study the evolutionary status of the analyzed region and have been successfully applied both to nearby irregular galaxies (Marconi et al. 1995) and to galactic open clusters (Bonifazi et al. 1990, Gozzoli et al. 1996, Bragaglia et al. 1997).

Our sample of old open clusters includes NGC2243 (age $\simeq 3$ Gyr, metallicity two tenths solar, Bonifazi et al. 1990), Collinder 261 (age $\gtrsim 7$ Gyr, almost solar metallicity, Gozzoli et al. 1996) and NGC6253 (age $\gtrsim 3$ Gyr, metallicity about twice solar, Bragaglia et al. 1997).

To them we add now NGC 2506, a moderately old open cluster already studied by McClure et al. (1981, hereinafter MCTF) and Chiu & van Altena (1981, hereinafter CvA), located toward the galactic anticentre ($\alpha_{1950} = 7^h 57.6^m$, $\delta_{1950} = -10^\circ 39'$; $l_{II} = 231^\circ$, $b_{II} = +10^\circ$). In section 2 we describe the observations and data analysis; in Section 3 we present the derived CMDs involving U,B,G,V,R,I photometry and discuss the presence of binary stars. In Section 4 we compare observed and synthetic CMDs and derive metallicity, age, distance and reddening. Finally, our findings will be discussed in Section 5.

2 OBSERVATION AND DATA REDUCTIONS

Images of the cluster were obtained during two separate observing runs, in 1985 and 1993, with telescopes located on Cerro Tololo and Mt. Palomar respectively (see Table 1). The total field covered is shown in Fig. 1.

[★] Based on observations made at CTIO and Mt. Palomar telescopes. CTIO is operated by the Association of Universities for Research in Astronomy under agreement with the National Science Foundation.

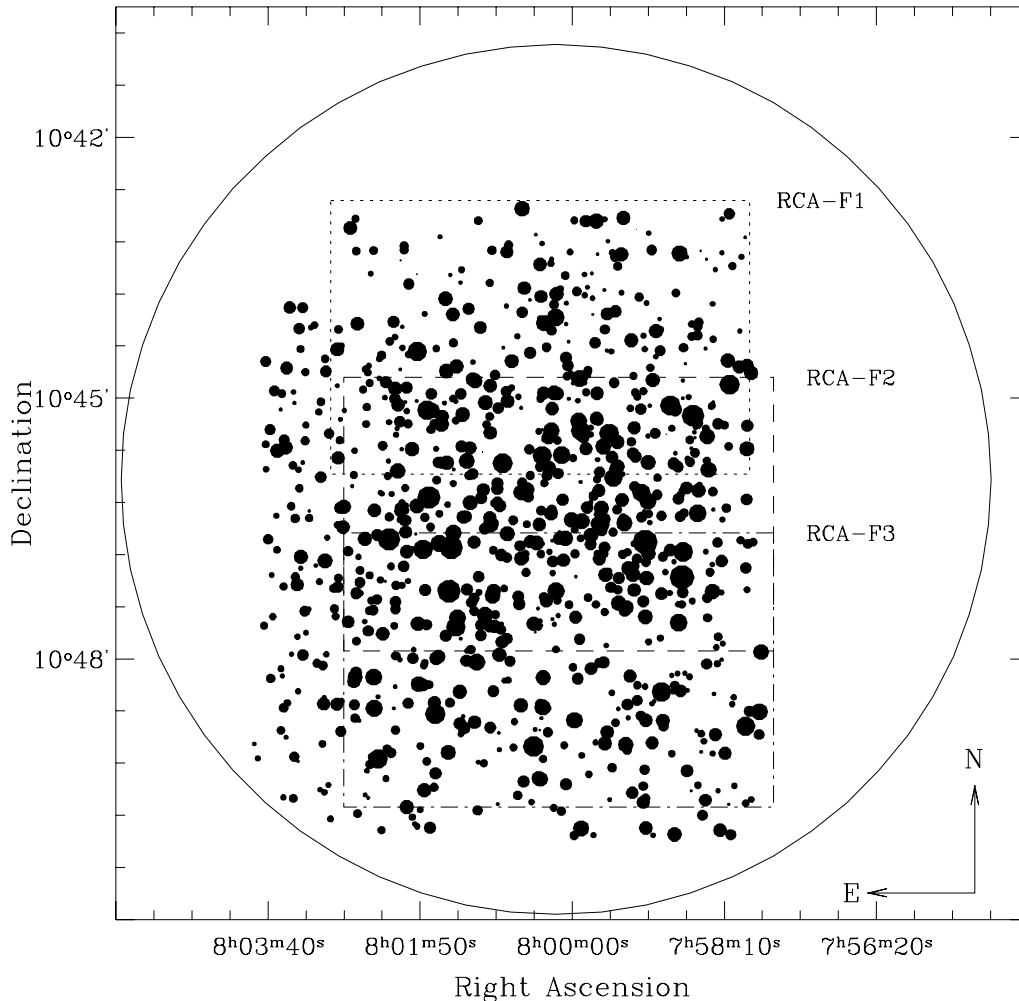


Figure 1. Map of the observed region of NGC 2506, from our photometry. Pixel coordinates have been transformed to equatorial coordinates (year 2000) making use of a set of stars identified on the Digitized Sky Survey. The circle indicates the field observed by MCTF and has a diameter of 10 arcmin

2.1 Observations

The first run was at the CTIO Blanco 4m telescope using the prime focus CCD camera with RCA2. The chip had good quantum efficiency even in the near-UV/blue, but a large read-out noise ($90 e^-$ rms). Using the doublet corrector, this CCD at prime focus yielded a spatial sampling of 0.58 arcsec per pixel.

Although this particular observing run consisted of several nights, the cluster was observed for only two of these nights, both of which were photometric. A minimum of 12 standard stars, as established by Graham (1982) and by Landolt (1983), were observed several times each night and through a range of airmass (1 to 2). The colours of the observed standard stars spanned from $B-V=-0.25$ to $B-V=1.35$, encompassing the whole range of colours found in the cluster members. The cluster observations were generally performed near the meridian, and never with an airmass more than 1.2.

The filters used for the observations (UBGVRI) con-

sisted of an unusual mixture of passband definitions. The passbands of B and V were defined by standard combinations of Schott coloured-filter glass. The passbands of R and I were defined by interference filters, common to CTIO/KPNO at that time. The U and G filters were those of Hamilton (unpublished). The U filter used in this case was a combination of Schott UG5 with a liquid copper sulfate cut-off. Schott UG5 is slightly redder and broader than the more standard UG2 commonly used at CTIO since 1985. The G filter was specially designed to be a reasonable representation of the passband defined by hypersensitized IIIaJ emulsions with a two mm thick Schott GG385 filter, with two slight modifications. The cut-on point was moved redward to 4150 \AA so as to clearly miss the influence of the 4000 \AA break, and the cut-off point was moved slightly blueward so as to reduce the contribution of bright night sky lines such as Hg 5460 \AA and [OI] 5577 \AA on the overall detected sky background. The measured passband has a width of about 1000 \AA and a central wavelength of $\sim 4750 \text{ \AA}$.

Table 1. Observing dates and filter sets

Date	Telescope, CCD	FOV	Filters
22-23/12/1985	CTIO 4m, RCA	3' × 5'	UBGVRI
30-31/03/1993	Palomar 60in, Tek	6' × 6'	BV

As the field-of-view of this CCD was rather small by modern standards (about 3' × 5'), the central part of the cluster was mapped with three fields, each slightly overlapping with its neighbour (see Fig. 1). Exposure times for the various frames varied from two seconds for the redder pass-bands to 150 seconds for the ultraviolet exposures. At each pointing of the telescope, several frames were taken in each filter. These data were later co-added, and it was this co-added frame that was analyzed. These short exposures were necessary so that the bright giants of this cluster would not exceed the dynamic range of the CCD.

The second observing run was conducted at the Palomar 60-inch telescope. The detector used was a thinned, back-side illuminated Tektronix 1024 × 1024 CCD at the Ritchey-Chrétien focus of this telescope. In this case, the filters used were only B and V and these were defined similarly as those used during the first observing run. The spatial sampling for this telescope/detector combination was 0.37 arcsec per pixel (field of view about 6' × 6'). The CCD data were not binned. The exposure times were 300 seconds each for all frames, except for several of those taken at the cluster centre, which were 100 seconds long. Two series of 6 fields extending due northward and due eastward from the cluster centre were taken, but here we only concentrate on the central frame.

2.2 Reductions

Basic CCD reduction of bias and dark current subtraction, trimming, flatfield correction were applied. Several frames of comparable seeing were co-added to obtain the deepest frames in each band for the RCA data set. The co-added frames as well as the single short exposures were analyzed. We applied the usual procedure for PSF study and fitting available in DAOPHOT-II (Stetson 1992) in MIDAS environment to all frames. The deepest V frame of each field has been used to search for stellar objects, setting the minimum photometric threshold for object detection at 6σ above the local sky background. All the objects identified in V were then fitted in all the other bands. The internal errors were estimated by computing the *rms* frame-to-frame scatter of the magnitudes obtained for these stars, following the precepts of Ferraro et al. (1990). The mean errors in B and V are shown in Table 2.

2.3 Photometric calibrations

Calibrations for the RCA data-set were carried out by a set of programs written by Dr. Peter Stetson (unpublished; private communication 1985). Errors in the fitted coefficients were generally less than 0.02 mag. The nightly scatter was quite small for BGVR, and somewhat higher for

Table 2. Mean errors for the magnitude bins

mag bin	Error B	Error V
<17.0	0.004	0.010
17.0-17.5	0.010	0.020
17.5-18.0	0.013	0.030
18.0-18.5	0.017	0.035
18.5-19.0	0.020	0.065
19.0-19.5	0.023	0.095
19.5-20.0	0.045	0.150

U and I. The coefficients for the various colour terms were from an average over this particular observing run, as were the second-order extinction coefficients. However, the zero-point and first order extinction coefficients varied sufficiently from night-to-night that these were determined separately for each night, assuming the aforementioned averaged coefficients. The resulting calibration equations are the following, where the lower case symbols refer to the observed quantities, the upper case to the tabulated magnitudes, and A stands for the airmass:

$$u = U + 1.470 - 0.333(U - B) + 0.410A - 0.075(U - B)A$$

$$\text{Nightly Scatter} = 0.035 \text{ mag}$$

$$b = B - 0.069 + 0.035(B - V) + 0.310A - 0.090(B - V)A$$

$$\text{Nightly Scatter} = 0.007 \text{ mag}$$

$$g = G - 0.345 - 0.091(B - V) + 0.192A + 0.028(B - V)A$$

$$\text{Nightly Scatter} = 0.0035 \text{ mag}$$

$$v = V + 0.154 - 0.042(B - V) + 0.150A + 0.050(B - V)A$$

$$\text{Nightly Scatter} = 0.009 \text{ mag}$$

$$r = R + 0.13 + 0.12A$$

$$\text{Nightly Scatter} = 0.018 \text{ mag}$$

$$i = I + 1.62 + 0.07A$$

$$\text{Nightly Scatter} = 0.033 \text{ mag}$$

For the P60 data set, though taken under photometric conditions, no photometric standards were observed, as another program had priority. These frames were calibrated from the photometric results of the first observing run as there was sufficient overlap to be able to define the transformation equations accurately.

Final results of the reductions yielded magnitudes for 863 stars in the composite sample. The table with UBGVRI magnitudes, coordinates, and cross-identification with MCTF is available from the first author.

2.4 Completeness analysis

We tested our luminosity function in the V and B band for completeness, using the routine ADDSTAR in DAOPHOT-II. In short, we added to the original V and B frames a pattern of artificial stars ($\simeq 10\%$ of the total in each magnitude bin), at random positions. The frames were reduced in the same way described above. We considered as “recovered” only those stars found in their given position and

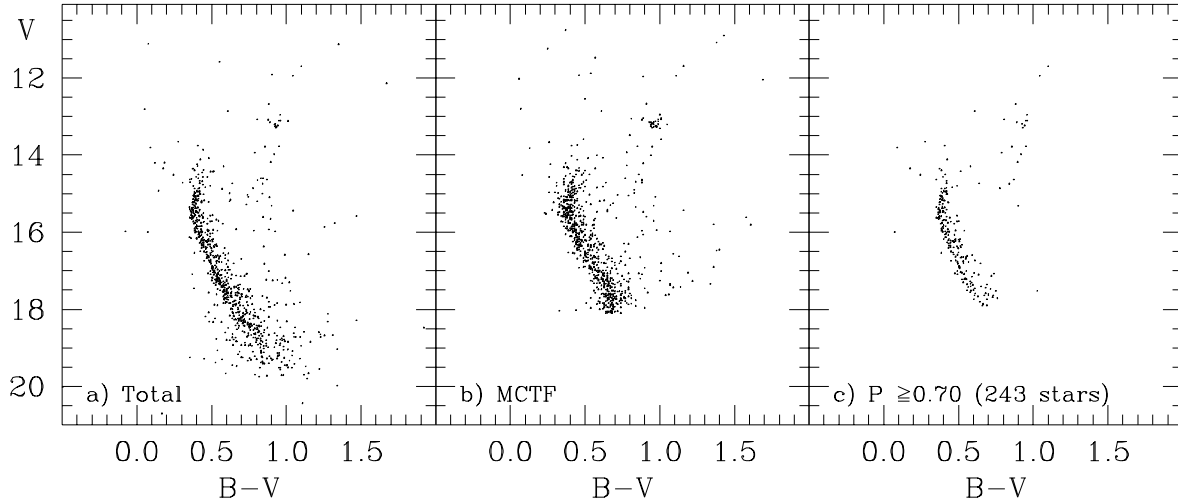


Figure 2. a) V , $B-V$ colour-magnitude diagram for the total sample (P60+RCA); all stars brighter than about the TO come only from the RCA chips. b) CMD taken from MCTF; notice the much larger spread of the MS. c) CMD for the P60+RCA data set, but only for stars with membership probability ≥ 0.7 .

Table 3. Completeness of our measurements in V and B , for the P60 field. Each value is the average of 30 trials, where 10 % of the total number of stars were added, following the luminosity function

Mag interv.	%V	%B
11.0-17.0	100	100
17.0-17.5	98	100
17.5-18.0	95	100
18.0-18.5	92	98
18.5-19.0	83	94
19.0-19.5	51	84
19.5-20.0	22	58
20.0-20.5	5	28
20.5-21.0	0	11

magnitude bin. The completeness was then derived as the ratio $N_{recovered}/N_{added}$ of the artificial stars generated. We performed 30 trials for band and the final averaged results are reported in Table 3.

3 THE COLOUR-MAGNITUDE DIAGRAMS

We present the colour-magnitude diagram (CMD) obtained from our reductions in Figs 2 and 3. Figs 2 refers to our total sample (P60+RCA frames), and is thus limited to the B and V filters. Fig. 3 instead contains only stars found in the three RCA fields, and diagrams are shown for various combinations of the UBGVRI filters.

Our V , $B-V$ diagram (Fig. 2(a)) agrees reasonably well with the one obtained by MCTF (Fig. 2(b)), but is much better defined. MCTF’s photographic study covered a diameter of 10 arcmin centred on the cluster, and our field is mostly contained in their zones I and II (see fig. 1 in

MCTF, and our Fig. 1). In Fig. 4 we show the differences between our magnitudes and theirs. These differences are less than 0.1 mag down to B or $V = 17$. However, there is a clear trend fainter than this, in the sense of our measures being $\lesssim 0.2$ mag brighter than those of MCTF.

Our Turn-Off (TO) point, defined as the bluest point of the top of the main sequence, is located at $V = 14.7$, $B - V = 0.35$. TO morphology* shows a definite “hook”, similar e.g. to the one in NGC6253 (Bragaglia et al. 1997), typical of an intermediate old age. The subgiant and red giant branches (SGB, RGB) are extended and well delineated. The red clump, which represents the locus of core-He burning stars, is found at $V = 13.2$, $B - V = 0.92$. There also are objects above the RGB, probably asymptotic branch stars; of them, at least 2 are cluster members (CvA, MCTF). At odds with many open clusters, NGC2506 does not seem to have a noticeable number of Blue Straggler Stars (see especially Fig. 2(c), where only probable cluster members are plotted).

Given the magnitudes of the TO and red clump, we derive $\delta V = V_{TO} - V_{clump} = 1.5$ which, following JP94 relation for the Morphological Age Index (MAI), suggests an age of 2.5 Gyr. We will see in section 4 that our derived age is actually younger.

3.1 The Lower Main Sequence

Our MS extends to about 2 mag fainter than that presented by MCTF. There appears to be a discrepancy with their diagram, as we see no blueward migration of the MS at these

* Proper interpretation of the TO morphology is complicated by the combination of the normal main sequence (MS) defined by single-stars, and by the binary sequence, which is 0.75 mag brighter than the normal MS. This binary MS is apparent in all the CMDs.

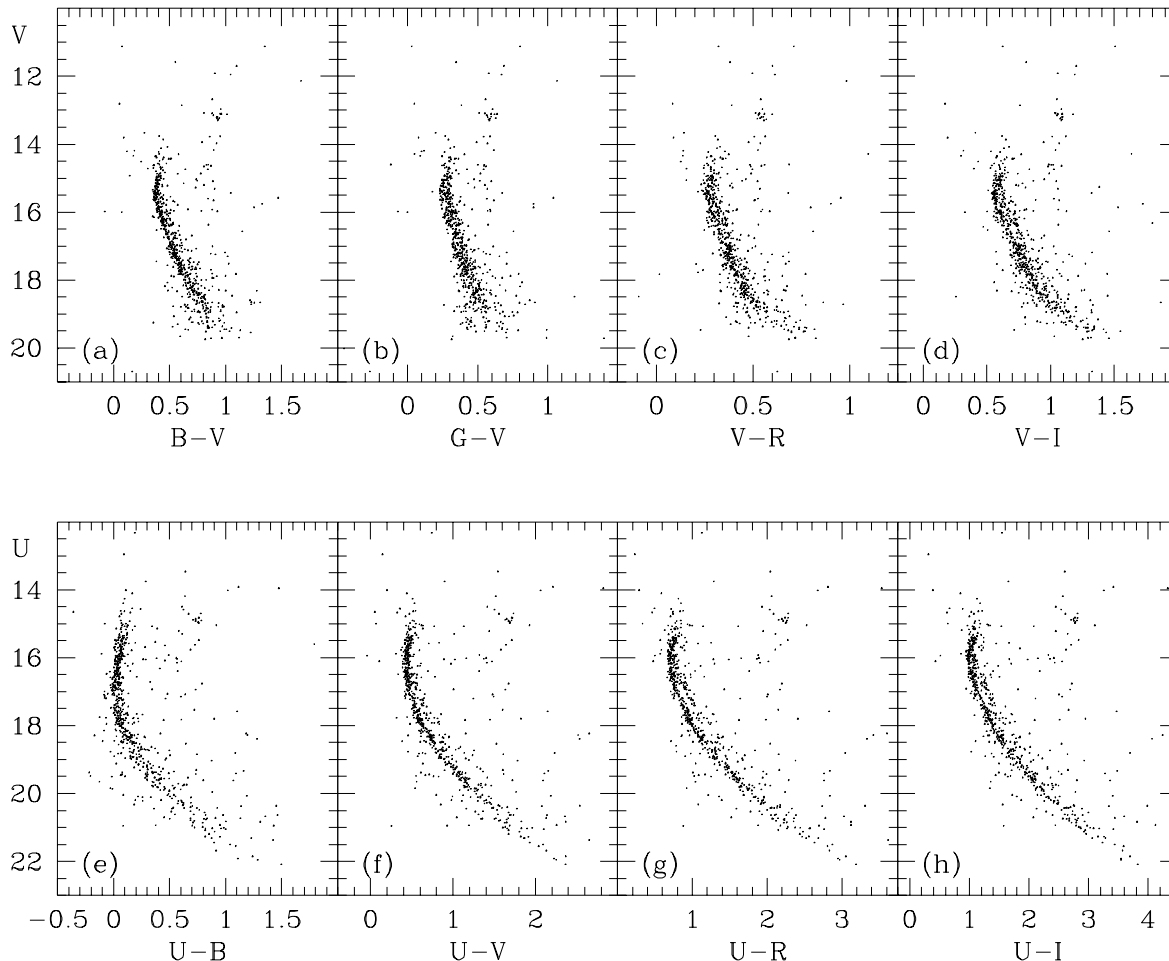


Figure 3. CMDs for the RCA sample alone: a) $V, B - V$; b) $V, G - V$, c) $V, V - R$; d) $V, V - I$; e) $U, U - B$; f) $U, U - V$; g) $U, U - R$; h) $U, U - I$

lower luminosities. We attribute such a peculiarity to non-linear effects in their photographic material near the plate limit.

Our cluster MS remains well defined also towards the faint end, though apparently increasingly less populated towards fainter luminosities. A similar effect had already been noticed by Scalo (1986), who used Chiu & van Altena’s data, and is not uncommon among open clusters. In this case, though, it seems to be perfectly explained by incompleteness in photometry at the faint limit (see Section 4 and Fig. 7). In other words, there is no indication of a flattening of the present-day mass function at the low-mass end, as seen in many other clusters (e.g. NGC6253, Bragaglia et al. 1997 or, as extreme case, NGC 3680, Nordstrom et al. 1996) and usually ascribed to dynamical evolution. This may be due to the Galactic position of the cluster. According to Carraro & Chiosi (1994b), who determined the orbit of this cluster using radial velocity information, NGC2506 has never moved very far away from its birthplace, having an orbit confined in distance from the Galactic centre between 10.7 and 11.6 kpc, and which doesn’t extend beyond 0.6 kpc from the Galac-

tic plane. Thus, NGC2506 has probably suffered less than other clusters from encounters with giant gas clouds which produce stripping of cluster members.

3.2 Field contamination

Field contamination is likely to be small in the anti-centre direction, but separation of field and cluster stars simply on the basis of photometry is neither easy nor unambiguous, since the cluster extends quite far (see Fig. 5 where panel a) corresponds to the cluster centre, and panels b) to e) to increasing distances). Even at about 30 arcmin from the centre there might be a slight cluster component mixed with the field stars. We will not discuss the cluster dimension and radial distribution, since these will be amply treated by Testa & Hamilton (1997).

Chiu & van Altena (1981) published a membership study of this cluster for the stars in MCTF; their table 2 contains 801 stars down to V about 18. Of the 863 stars in our catalogue, 462 were cross-identified with MCTF on the basis of position and magnitude, while 401, mostly faint,

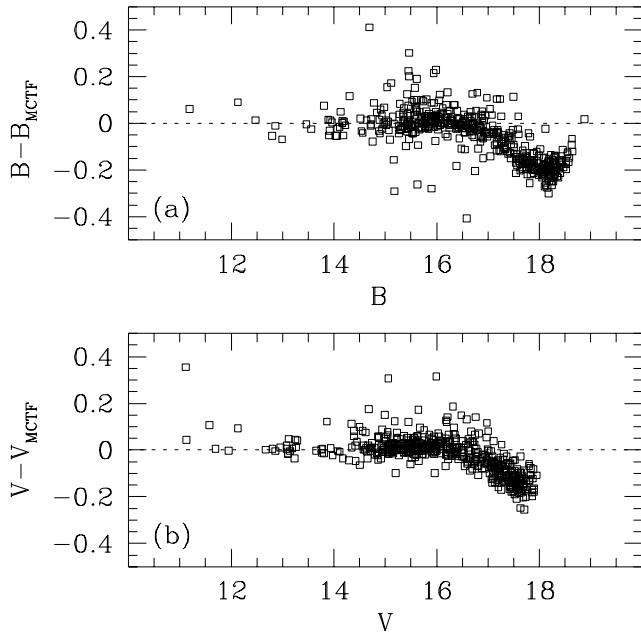


Figure 4. Comparison between MCTF’s and our photometry in B and V for the 462 stars in common (see Sect. 3.2)

are present only in our photometry. The synthetic CMDs described in section 4 will be compared to our whole sample, since we lack membership information for $V=18-20$ and there is no way to assess the incompleteness of the membership study at the faint limit. The CvA data are instead very useful at the bright end, since we can be sure of how the MS behaves near the TO, of the position of the subgiant and red giant branches, and of the location of the clump (see Fig. 2(c), where we show only those stars with membership probability ≥ 0.70).

3.3 Binary stars

Most open clusters show indications of a sizeable binary population, detected either spectroscopically (see e.g. Mermilliod & Mayor 1989, 1990) or photometrically (see e.g. M 67, Fan et al. 1996, or two clusters quite similar to NGC2506: NGC 2243, Bonifazi et al. 1990, and NGC 2420, Anthony-Twarog et al. 1990).

NGC2506 has been unsuccessfully surveyed for close/moderately close binaries in the past: Cameron & Reid (1987) found no candidate binary among 26 subgiant/lower red giant cluster members. Their technique was based on the detection of chromospheric emission in the CaII H+K lines due to enhanced axial rotation produced by orbital locking and was claimed to be sensible to periods of about 1 to 50 days. Kaluzny & Shara (1988) found no contact binaries of the W UMa type, with periods in the range a few hours – 1.5 days, in their CCD survey of 6 old open clusters, among which was NGC2506. MCTF, on the basis of the scatter of the MS, estimated a crude 50 % of binaries in NGC2506.

The $V, B - V$ diagram is not the most suitable to sep-

arate the secondary sequence due to binary systems from the single-star MS: much better resolution in colour is obtained in the CMD’s involving the U band (see Fig. 3). To quantify the visual impression of well populated binary star sequences, we have performed a simple experiment on RCA-F1, our best field both for photometric accuracy and crowding conditions, using the $U, U - I$ CMD. After defining a MS ridge line, we have measured the distance in colour of every star from this MS and plotted the distance histograms in four separate magnitude bins (see Fig. 6 – left panel – for a definition of the MS and magnitude intervals, and Fig. 6 – middle panel – for the histograms). A secondary peak in the colour distribution is clearly present: counting stars in it and in the “MS peak”, we derive a binary frequency of about 17 %. Finally, the right panel of Fig. 6 shows the histogram of the distance of each star in RCA-F1 from the MS ridge line: here too the secondary peak is clearly prominent.

This value is referred to the central part of the cluster, but since NGC2506 does not suffer from segregation of the more massive objects toward the centre, as seen from the luminosity function (Fig. 7), we may assume it is representative of the cluster as a whole.

4 CLUSTER PARAMETERS

In the case of NGC2506, there are estimates within the literature of the age, reddening and metallicity, with the latter two being fairly reliable: MCTF derived $E(B-V)=0.05$ from photoelectric measures and Friel & Janes (1993) obtained $[Fe/H]=-0.52 \pm 0.07$ from medium-resolution spectroscopy of 5 cluster members.

To derive our own values for these parameters, we have applied to NGC2506 the approach of CMD simulations described by Tosi et al. (1991). This technique has been employed for three other old open clusters (Bonifazi et al. 1990, Gozzoli et al. 1996, Bragaglia et al. 1997). Due to the existing estimate of the cluster metal content, we have restricted the sample of stellar evolution tracks adopted to construct the synthetic CMDs to those sets with metallicities near that value. The major features of these sets are summarized in Table 4 where their origin is also given. For each set of stellar models, we have performed several MonteCarlo simulations for any reasonable combination of age, reddening and distance modulus.

The incompleteness factors and the photometric errors in each magnitude bin assigned to the synthetic stars in each photometric band are those derived from the observed data and mentioned in section 2. Naturally, the number of stars in the synthetic diagram is the same as that in the empirical CMD of Fig. 2(a). To compare the model predictions with the observational distributions (both CMD and luminosity function, LF), we have taken into account the number of probable non members, estimated with the help of CvA’s diagrams with different membership probability. However, we have not removed any of the stars above the MS turn-off, and this is why the cluster LF (represented by the open circles in the bottom panel of Fig. 7) is always slightly higher than the curve predicted by the models in the brightest magnitude bins.

Since the data show evidence for a significant fraction of binary stars among the cluster members, we have taken

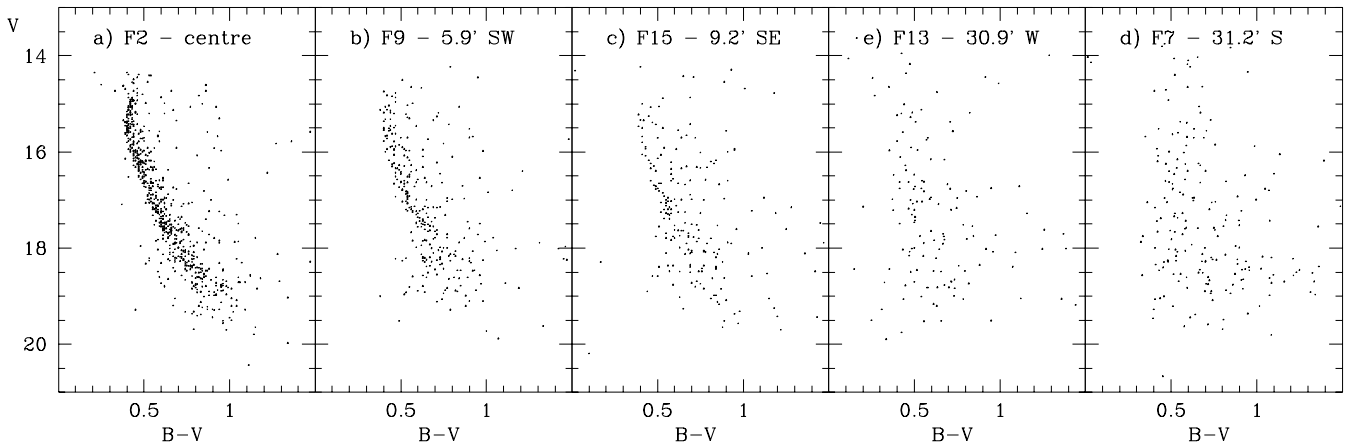


Figure 5. CMD for the MS, derived from P60 fields, at increasing distance from the cluster centre, shown in panel a). The other CMDs are for areas distant respectively: b) 6 arcmin, c) 9 arcmin, d) and e) 31 arcmin

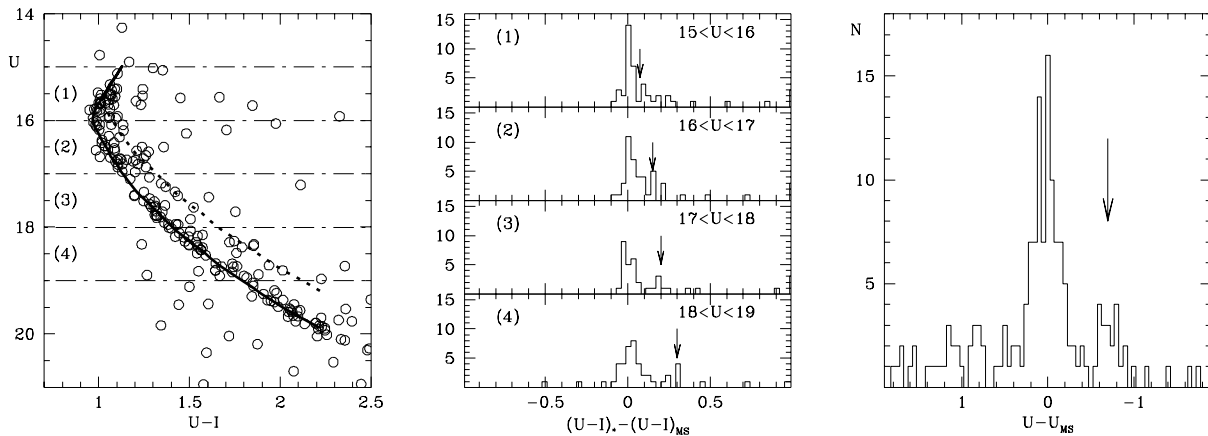


Figure 6. Left panel: $U, U - I$ CMD for stars on/near the MS in the RCA-F1 field; the MS ridge line and a secondary sequence 0.7 mag above it (representing the equal-mass binary systems) are also shown. Middle panel: histograms of the distance in colour from the MS ridge line of all stars, divided in 4 magnitude intervals; the arrows indicate roughly the position of the equal-mass binary sequence in the middle of each mag bin, as measured from the left panel. Right panel: histogram of the magnitude distance from the MS ridge line; the arrow indicates the position of stars 0.7 mag brighter than this line.

Table 4. Stellar evolutionary tracks adopted for the synthetic CMDs

Model	Y	Z	M_{min} (M_{\odot})	M_{max} (M_{\odot})	Reference	Notes
FRANEC	0.27	0.01	0.6	9	Castellani et al. 1993	to AGB-tip, LAOL op.
FRANEC	0.27	0.02	0.6	9	Castellani et al. 1993	to AGB-top, LAOL op.
Geneva	0.26	0.008	0.8	120	Schaerer et al. 1993	only to RGB-tip
Geneva	0.30	0.02	0.8	120	Schaller et al. 1992	Charbonnel et al. 1996 for e-AGB
Padova	0.28	0.008	0.6	120	Alongi et al. 1993	to AGB-tip
Padova	0.28	0.02	0.6	120	Bressan et al. 1994	to AGB-tip

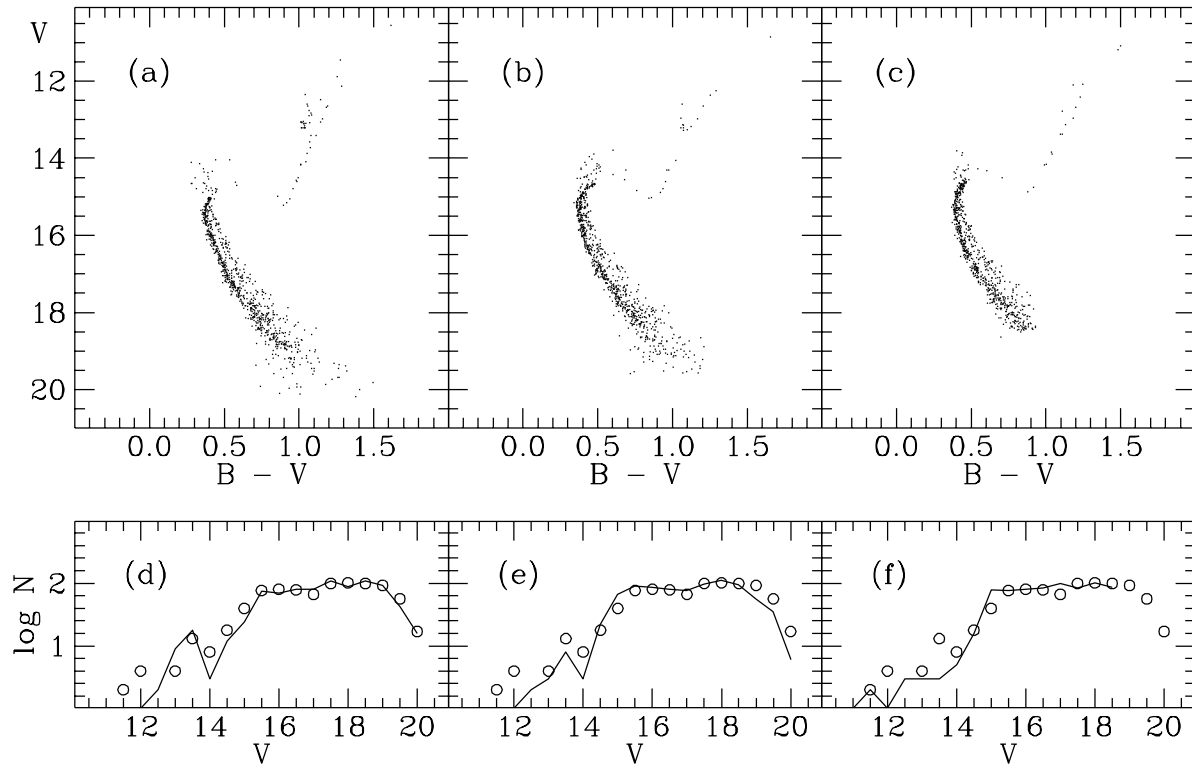


Figure 7. Models in better agreement with the data: the synthetic CMDs (to be compared with that in Fig. 3(a)) are in the top panels and the corresponding luminosity functions in the bottom panels (lines for the models and open circles for the data). Panels (a) and (d) correspond to FRANEC with $Z=0.01$, panels (b) and (e) to Padova with $Z=0.02$, and panels (c) and (f) to Geneva with $Z=0.008$. See text for details.

them into account in the synthetic diagram. A mass ratio has been associated to each system via random extractions from a flat distribution. We have then followed the prescriptions given by Maeder (1974) to attribute colours and magnitudes to systems with different primary/secondary mass ratios (see Bragaglia et al. 1997 for more details). It is interesting to notice that all the stellar models lead to synthetic CMDs in better agreement with the data when the assumed fraction of binaries is 30%. As already discussed by Maeder (1974) and Fan et al. (1996), this percentage is larger than that derived by counting the stars on the right side of the MS (see section 3.3) and the difference is due to the combination of several selection effects.

We wish to note here that *all* of the simulated cases yield red-giant branches that are slightly redder than the observed ones and that in all cases, except in the FRANEC models with $Z=0.02$, this colour excess is already visible at the base of the RGB. We ascribe this effect to the uncertainty in the photometric conversions from the theoretical plane (luminosity and effective temperature) to the observational one (magnitude and colour): the temperature-colour conversion is the one that is most affected. The fact that, at the same colours, the discrepancy is not observed in the lower MS (except perhaps in the Padova models with $Z=0.02$) suggests that the inadequacy of the temperature-

colour conversion does not concern all the cool stars, but only those in low-gravity conditions, a circumstance foreseen by Bessel et al. (1989).

4.1 Results with FRANEC stellar models

Both of the examined sets of FRANEC evolutionary tracks provide synthetic CMDs and LFs in agreement with the observed data, although with slight differences in the choices of the parameters. With the set at $Z=0.01$, the best fit is obtained assuming an age of 1.6 Gyr, a reddening $E(B-V)=0.07$ and a distance modulus $(m-M)_0=12.6$. As shown in panels (a) and (d) of Fig. 7 these stellar models reproduce quite well all the observed features of the cluster (namely: the magnitude and colour distribution of the stars, the relative number of stars in the various evolutionary phases and their morphology, including the MS gaps).

A very good agreement with the data, practically indistinguishable from that shown in Fig. 7 (a) and (d), is achieved also with the FRANEC set with $Z=0.02$. In this case, the best model indicates roughly the same age (1.5 Gyr) and distance modulus ($(m-M)_0=12.7$), but a lower reddening ($E(B-V)=0.01$), to compensate the intrinsically redder colours corresponding to the doubled metallicity. These tracks have a metal content nominally larger than that spec-

troscopically attributed to NGC2506. However, according to their authors, the FRANEC tracks (i.e., both the set with $Z=0.01$ and with $Z=0.02$) actually correspond to models with metallicity about half of their nominal value, once the effect of using the old LAOL opacities rather than the most recent OPAL opacities is taken into account. Both sets are, therefore, roughly compatible with the spectroscopic metallicity $[\text{Fe}/\text{H}]=-0.5$ derived by Friel & Janes (1993).

4.2 Results with Padova stellar models

The stellar evolutionary models computed by the Padova group are slightly brighter than the corresponding FRANEC models, probably because they take into account the possible overshooting from the convective core, and a larger core implies higher brightness. For this reason, the ages derived from overshooting models are usually older than those derived with standard treatment of the convective regions. The luminosity difference between FRANEC and Padova models can be appreciated comparing panels (a) and (b) of Fig. 7: in both cases the faintest stars have mass $0.6 M_{\odot}$, but they appear brighter in the Padova than in the FRANEC diagram. Notice also the rounder shape of the MS turn-off region of the Padova CMDs.

In the case of NGC2506, the age difference is, however, very small. With the Padova tracks with $Z=0.008$, the best fit to the cluster features is obtained for an age 1.7 Gyr and assuming $E(B-V)=0.05$ and $(m-M)_0=12.5$, confirming that the literature reddening is the most appropriate when the cluster is assigned the spectroscopic metallicity.

It must be emphasized, however, that an equally good fit is attained with the Padova solar metallicity models, in which case the reddening must be smaller to compensate for the intrinsic redder colour of more metal rich stars. The best case for $Z=0.02$ assumes $E(B-V)=0.0$, $(m-M)_0=12.6$, an age of 1.7 Gyr, and is shown in Fig. 7 (b) and (e). Notice that the metallicity significantly affects only the reddening determination.

These results are in striking agreement with those derived from the FRANEC models described above. This shows that in the mass range of the stars in NGC2506 (stars at the MS turn-off have masses $1.7-1.9 M_{\odot}$) the overshooting effect on the age of the stellar models is moderate.

4.3 Results with GENEVA stellar models

The Geneva stellar models take into account the overshooting off convective cores, although with a formalism different from that applied in the Padova tracks. For a given stellar mass, these are the brightest models of the various sets examined here and should provide the oldest age.

Figs 7 (c) and (f) show the Geneva model in better agreement with both the CMD and the LF of NGC2506: with $Z=0.008$, it indicates an age of 2.2 Gyr and requires $E(B-V)=0.05$ and $(m-M)_0=12.5$. The helium burning phases have not been computed for the Geneva stellar tracks with this metallicity. They provide a lower number of post-MS stars than the FRANEC and Padova models and the clump is not visible. This leads to a worse reproduction of the empirical LF in the magnitude bins brighter than $V \simeq 14$. The absence of the predicted curve in the faintest

Table 5. Summary of best-fits results for distance modulus, age, and reddening for all models used

Model	Z	$(m-M)_0$	τ (Gyr)	$E(B-V)$
FRANEC	0.01	12.6	1.6	0.07
FRANEC	0.02	12.7	1.5	0.01
Padova	0.008	12.5	1.7	0.05
Padova	0.02	12.6	1.7	0.00
Geneva	0.008	12.5	2.2	0.05
Geneva	0.02	12.5-12.6	1.7-2.0	0.00

magnitude bins (Fig. 7(f)) is due to the fact that the Geneva stellar evolutionary tracks have been computed only for stars more massive than $0.8 M_{\odot}$ and should not be taken as a model failure.

The Geneva tracks with solar metallicity have instead been computed also for the later evolutionary phases and show the clump in the right CMD position. However, they provide in general a worse reproduction of the cluster features, probably because of their excessive metallicity. The derived parameters are, however, consistent with the others: the age is in the range 1.7-2.0 Gyr, $E(B-V)=0.0$ and $(m-M)_0=12.5$ or 12.6.

5 SUMMARY AND DISCUSSION

We have determined for NGC2506 a confidence interval for distance, age, reddening and metallicity (see Table 5).

a) Distance: in all our trials with the six sets of models we have a best fit for $(m-M)_0$ in the range 12.5 – 12.7. This is to be compared with the 12.2 value found by MCTF using the Ciardullo & Demarque (1977) isochrones. We must emphasize that with none of our models are we able to provide a stellar distribution in the CMD compatible with the data with such a low distance modulus. CC94 have derived $(m-M)_0=12.5$, which is in agreement with our derivation.

b) Age: it varies from 1.5 to 2.2 Gyr depending on the adopted set of stellar evolutionary models, with better fits for ages 1.5-1.7 Gyr. This value is much smaller than the 3.4 Gyr derived by MCTF and the 6 Gyr found by Bararo & Pigatto (1984). Only part of the age overestimates of those studies is attributable to their adopted shorter distance, which naturally implies lower intrinsic brightness and, therefore, older age. Most of the problem resides in the use of the isochrone fitting method with older, less accurate, stellar models combined with the uncertainty in the definition of the MS turn-off (fig.6 in MCTF clearly shows that what we have considered as the turn-off is closer to their 2 Gyr than to the 3 Gyr isochrone). Our age is also smaller than the 2.5 Gyr cited in Friel (1995), and based on the MAI defined by JP94: this point will be shortly discussed later. It is instead in excellent agreement with the 1.9 Gyr found by CC94, who used the same distance modulus and Padova tracks adopted here.

c) Reddening: it strongly depends on the metallicity of the models, but varies from 0 to 0.07, in good agreement with the 0.05 value found by MCTF.

d) Metallicity: we have obtained excellent fits using the sets of models with metal content lower than solar, in agree-

ment with the spectroscopic value. However, in one case (Padova models), we have also reached satisfying results with the solar metallicity set. This is because a tight determination of the metallicity cannot be done on the basis of the photometry alone. While spectroscopic values are to be preferred in general, we remind that the $[\text{Fe}/\text{H}]=-0.52$ found by Friel & Janes (1993) is based on medium-low resolution spectra, calibrated against a metallicity scale. High resolution direct spectroscopy will be able to put a more stringent limit on metallicity, and our $V - I$ values could be used to derive input temperatures for the model fitting analysis.

As a by-product of our theoretical simulations, we can also provide a lower limit to the initial mass of the cluster within the examined region; that is the minimum mass of the stars that must have formed there to account for the current stellar content. This value turns out to be $\langle M_i \rangle \simeq 2.6 \times 10^3 M_\odot$ (ranging from 1.6 to 3.0 depending on the adopted evolutionary tracks) and is a lower limit to the actual initial mass of the cluster region, since it does not take into account the possible effect of subsequent stellar evaporation.

The age differences presented at point b) show, in our opinion, how much safer it is to date the clusters with the synthetic CMDs rather than with isochrone fitting. Both methods provide results dependent on the adopted stellar evolution models. However, the synthetic CMDs, on the one hand, are independent of any other parameter and, on the other, are constrained by the many morphological features (e.g., shape of the MS, SG and RG branches, position of the clump, of the TO, of the MS gaps), by the stellar distributions with magnitude and colour in the diagram, and by the proportion between stars in different evolutionary phases. Isochrone dating is strongly affected by the choice of the MS turn-off (which can be quite subjective) and has no further constraint aside from the average stellar distribution in the CMD. Besides, it cannot account for the colour and magnitude spread due to photometric errors or for the effect of incompleteness on the relative number of stars in the various phases.

Our study of open clusters is aimed at better understanding the chemical and dynamical evolution of the Galaxy; as stated in the Introduction, their ages (and distances) are among the soundest derived for the disc population. Nevertheless, homogeneity in dating them is fundamental if one wishes to preserve a meaningful age ranking.

In this respect, the effort made by CC94, who re-analyzed ten well observed clusters and defined a relation between a measurable index (ΔV) and age, is very important. Carraro & Chiosi defined ΔV as the difference in magnitude between the TO and the red clump (like the δV used by JP94), but taking into account the possible misplacement of the TO due to the binary sequence by adding an extra 0.25 mag to the value found from the CMD. They have then derived the age of the ten clusters with the synthetic CMD method and obtained a linear fit between $\text{Log}(\text{age})$ and ΔV . They have then applied this relation to derive ages for a sample of 26 clusters with reliable photometry published.

JP94 used a similar approach. They used literature values for ages (stressing the fact that in doing so they lacked the homogeneity one would have wished for), and chose the 7 more reliable open clusters. They derived a non-linear relation between δV and $\text{Log}(\text{age})$, using also values for Glob-

Table 6. Comparison of ages derived for our sample of old clusters, from MAI (JP94) and by CC94

Cluster	τ (Gyr)	δV (mag)	MAI (Gyr)	ΔV (mag)	CC94 (Gyr)
NGC2506	1.5-2.2	1.5	2.5	1.75	1.9
NGC6253	3.0	2.0	4.4		
NGC2243	3-5	2.2	5.6	2.15	4.5
Cr261	7-11	2.6	9.5		

ular clusters. In this way their relation is quite sound for high δV values, and furthermore, these are intrinsically simpler to measure, since for older ages the red clump is more populated, hence easier to locate precisely. At intermediate ages, like in the case of NGC2506, there seems instead to be a discrepancy (see Table 6), with ages from δV too high. The same problems exists for the CC94 relation (their eq. 3): their measured $\Delta V=1.75$ for NGC2506 yields an age of about 2.5 Gyr, which decreases to 1.8 Gyr using instead 1.5 (our value).

Comparing CC94's ΔV and JP94's δV for the 26 clusters common to CC94 and JP94, one finds a mean difference of about 0.15 mag, in the sense of larger values for CC94. Restricting the comparison to the 6 clusters in common chosen among the 7 best clusters used by JP94 to build the MAI relation yields a mean difference of 0.25 mag (excluding the case of NGC3680, a scarcely populated cluster, for which the difference is 0.7 mag). For these 6 objects the mean age difference is about 0.1 Gyr. We then conclude with this *caveat* about the MAI age ranking system, which could lead to conspicuous errors in individual ages. The effort to build a more refined relation is huge, but worth pursuing.

ACKNOWLEDGEMENTS

The bulk of the numerical code for CMD simulations has been provided by Laura Greggio. The FRANEC, Geneva and Padova evolutionary tracks were kindly made available by their authors. The authors would like to thank Dr. Neill Reid for a critical reading of the manuscript and Dr. Vincenzo Testa for help with various aspects of the photometric reductions. We made use of the digitization of photographic data obtained at the UK Schmidt Telescope (Digitized Sky Survey, produced at the Space Telescope Science Institute under US Government grant NAG W-21). This research has made use of the Simbad database, operated at CDS, Strasbourg, France.

REFERENCES

- Alongi, M., Bertelli, G., Bressan, A., Chiosi, C., Fagotto, F., Greggio, L., Nasi, E. 1993, AAS, 97, 851
- Anthony-Twarog, B.J., Kaluzny, J., Shara, M.M., Twarog, B.A. 1990, AJ, 99, 1504
- Barbaro, G., Pigatto, L. 1984, A&A, 136, 355
- Bessel, M.S., Brett, J.M., Scholz, M., Wood, P.R. 1989, AAS, 77, 1
- Bonifazi, A., Fusi Pecci, F., Romeo, G., Tosi, M. 1990, MNRAS, 245, 15

- Bragaglia, A., Tessicini, G., Tosi, M., Marconi, G., Munari, U. 1997, MNRAS, 284, 477
- Bressan, A., Fagotto, F., Bertelli, G., Chiosi, C. 1994, AAS 100, 647
- Cameron, A.C., Reid, N. 1987, MNRAS, 224, 821
- Carraro, G., Chiosi, C. 1994a, AA, 287, 761, CC94
- Carraro, G., Chiosi, C. 1994b, AA, 288, 751
- Castellani, V., Chieffi, A. & Straniero, O. 1993, ApJS 78, 517
- Charbonnel, C., Meynet, G., Maeder, A., Schaerer, D. 1996, A&AS 115, 339
- Chiu, L.-T.G., van Altena, W.F. 1981, ApJ, 243, 827
- Ciardullo, R.D., Demarque, P. 1977, Trans. Yale Univ. Obs, 33, 1
- Fan, X., et al 1996, AJ, 112, 628
- Ferraro, F.R., Clementini, G., Fusi Pecci, F., Buonanno, R., Alcaïno, G. 1990, A&AS, 84, 59
- Friel, E.D. 1995, ARAA, 33, 381
- Friel, E.D., Janes, K.A. 1993, AA, 267, 75
- Gozzoli, E., Tosi, M., Marconi, G., Bragaglia, A. 1996, MNRAS, 283, 66
- Graham, J.A. 1982, PASP, 94, 244
- Janes, K.A. 1979, ApJS, 39, 135
- Janes, K.A., Phelps, R.L. 1994, AJ, 108, 1773, JP94
- Kaluzny, J., Shara, M. 1988, AJ, 95, 785
- Landolt, A.U. 1983, AJ, 88, 439
- Maeder, A., 1974, A&A, 32, 177
- Marconi, G., Tosi, M., Greggio, L., Focardi, P. 1995, AJ, 109, 173
- McClure, R.D., Twarog, B.A., Forrester, W.T. 1981, ApJ, 243, 841
- Mermilliod, J.C., Mayor, M. 1989, A&A, 219, 125
- Mermilliod, J.C., Mayor, M. 1990, A&A, 237, 61
- Nordstrom, B., Andersen, J., Andersen, M.I. 1996, A&AS, 118, 407
- Panagia N., Tosi M. 1981, A&A, 96, 306
- Sandage, A.R. 1988, A.G.D. Philip, L. Davis, eds, Calibration of stellar ages, (Schenectady USA), p.43
- Scalo, J.M. 1986, Fund.Cosm.Phys. 11, 1
- Schaerer, D., Meynet, G., Maeder, A., Schaller, G. 1993, A&AS 98, 523
- Schaller, G., Schaerer, D., Meynet, G., Maeder, A., 1992, A&AS 96, 269
- Stetson, P.B. 1992, User's Manual for DAOPHOT-II
- Testa, V., Hamilton, D. 1997, in preparation
- Tosi, M., Greggio, L., Marconi, G., Focardi, P. 1991, AJ, 102, 951